

Dynamic In-hand Sliding Manipulation

Jian Shi, J. Zachary Woodruff, and Kevin M. Lynch

Abstract—This paper presents a framework for planning the motion of an n -fingered robot hand to create an inertial load on a grasped object to achieve a desired in-grasp sliding motion. The model of the sliding dynamics is based on a soft-finger limit surface contact model at each fingertip. The framework is applied to the problem of regrasping a block held in a pinch grasp. The approach is applied to two examples in simulation, one of which is tested experimentally.

I. INTRODUCTION

A. Background

Most human, animal, and even robot manipulation tasks involve controlling motion of the object relative to the manipulator, particularly in nonprehensile (grasplless) manipulation modes such as pushing, rolling, pivoting, tipping, tapping, and kicking. Even in pick-carry-place manipulation, where the carry portion of the task keeps the object stationary relative to the hand, the pick and place phases typically involve the object sliding or rolling on the fingers as the hand achieves a firm grasp or lets the object go. Other examples of controlled relative motion in grasping manipulation include finger gaiting, where the fingers quasistatically walk over the object to achieve a regrasp, all the while maintaining a stable grasp; rolling the object on the fingertips; and letting the object slide relative to the fingertips. Together these may be referred to as in-hand manipulation.

We are studying controlled sliding in a grasp for three purposes:

1) *Error-corrective sliding in an assembly task.* The problem is to choose a grasp configuration satisfying force-closure constraints as well as providing error-corrective sliding motion in response to likely disturbance forces during the place operation. For example, uncertainty in a peg-in-hole assembly task results in contact forces that should be mapped to error-corrective motion, such as using the springs of the RCC device [1] or using active accommodation control [2]. Instead, it is possible to use sliding at the fingertips as the source of compliance. By the choice of finger locations and normal forces, we can control the shape of the grasp *limit surface* (Sections II and V), which governs the mapping from contact forces to sliding directions, much like an accommodation control law maps contact forces to corrective velocities.

Jian Shi, J. Zachary Woodruff, and Kevin M. Lynch are with the Neuroscience and Robotics Lab (NxR), Northwestern University, Evanston, IL 60208 USA. {JianShi, jzwoodruff} at u.northwestern.edu, {kmlynch} at northwestern.edu. Kevin M. Lynch is also affiliated with the Northwestern Institute on Complex Systems (NICO).

This work was supported by NSF grant IIS - 0964665.

2) *Regrasping using external contacts.* In the previous task, the goal is to achieve a desired object configuration relative to external fixtures. In this task, the goal is to achieve a desired object configuration relative to the hand. Contact with the environment is used to provide forces that cause the object to slide relative to the fingers to a desired new grasping configuration. A manually designed example of this can be found in [3].

3) *Regrasping using dynamic loads.* In the previous task, the forces to cause the regrasp come from contact. In this task, the hand uses inertial forces on the object to cause it to slide to the desired new grasp by accelerating the hand beyond what the finger friction forces can support.

This paper focuses on the last problem: accelerating the hand to achieve a desired regrasp. Our testbed is the ERIN robot manipulation system, which consists of a 7-DOF Barrett WAM robot arm, a four-fingered Allegro robot hand outfitted with four SynTouch BioTac tactile sensing fingertips, and a 10-camera high-speed OptiTrack vision system as shown in Fig. 9 (a). Assuming the fingers are compliantly mounted, and the initial grasp configuration is chosen, research topics include:

- 1) given the state of the hand/object, the contact normal forces, and the acceleration of the hand, find the relative acceleration of the object (forward dynamics);
- 2) given the state of the hand and object and the desired relative acceleration of the object, find appropriate hand accelerations and contact normal forces (inverse dynamics);
- 3) planning the hand motion (and possibly contact normal forces) to achieve a desired regrasp;
- 4) iterating planning and execution of hand motions to iteratively reduce grasp error; and
- 5) real-time feedback control of hand motion and finger normal forces during sliding motion to achieve the desired regrasp;
- 6) estimation of friction properties from observed object motions, given the motion of the hand and the contact normal forces.

In this preliminary study, we use a simple unactuated hand in place of the Allegro hand and tactile sensors, and we focus on items 1)–4) above with constant normal force. In particular, we focus on the case of planar motion, where the object moves with three degrees of freedom (two translational and one rotational) and the fingers grasp the object on opposite sides that are parallel to the plane of motion. Friction property estimation and feedback control is out of the scope of this paper and will be addressed in future work.

B. Statement of Contributions

- 1) We have developed a framework for iterative planning of dynamic in-hand sliding for n -fingered planar regrasps.
- 2) We provide solutions to the forward and inverse dynamics problems using soft-finger contact models.
- 3) We have validated the approach with simulations and preliminary experiments.

C. Paper Outline

Section II reviews previous work on which this paper builds. In Section III we solve problems 1)–4) for a simple 1-DOF example. In Section IV we generalize the problem for an n -fingered grasp moving in a plane. In Section V we discuss the limit surface model for friction and derive expressions for the frictional force given a relative velocity between a rigid object and soft-finger contacts. In Section VI we derive the sliding dynamics and outline a method to calculate the acceleration of the object relative to each finger given the accelerations of the fingers. In Section VII we address the problem of planning the finger motion that achieves a desired regrasp for a given n -fingered grasp. In Section VIII we apply the motion planning approach to two example problems in simulation and we experimentally validate the results of one of the examples in Section IX.

II. RELATED WORK

A. In-hand Manipulation

There has been extensive work on kinematic in-hand manipulation where an object is moved relative to a finger without breaking contact or sliding on the surface. Trinkle and Hunter [4] extended the dexterous manipulation planning problem to consider rolling and slipping contact modes. The hybrid planning problem was further developed by Yashima et al. [5].

In-hand sliding manipulation can also be used to quickly reposition the object in the hand. Traditional dexterous regrasp methods such as finger gaiting or “place” and “pick” may be slow or not possible given the number of fingers or the surrounding environment. Brock addressed the problem of controlled sliding by first generating a constraint state map which outlines constraints on a grasped object due to the contact types and forces. By varying the contact forces he achieved controlled sliding in desired directions for a grasped cylinder [6].

Dynamic forces can also be used for in-hand manipulation. Furukawa et al. demonstrated regrasping by tossing a foam cylinder up and catching it [7]. Chavan-Dafle et al. tested hand-coded regrasps that take advantage of external forces such as gravity, dynamic forces, and contact with the environment to regrasp objects using a simple manipulator [3].

Arisumi et al. have explored the idea of casting manipulation where a manipulator is thrown and its “free flight” trajectory can be controlled in midair using tension forces in a tether [8]. Similarly, dynamic in-hand sliding motions allow the manipulator to impart forces on the object during

motion. This allows for feedback control and the ability to quickly and easily regrasp the object at any point throughout the trajectory.

B. Friction Modeling

Goyal et al. [9] describe the concept of a limit surface as a two-dimensional surface in a local three-dimensional force-moment space. The limit surface defines the set of external wrenches that can be resisted by the frictional forces due to the contact. Xydas and Kao [10] derived models of soft-finger contacts and the resulting limit surfaces.

III. 1-DOF EXAMPLE

In this section we solve research topics 1)–4) from the introduction for a simple 1-DOF example.

For the 1-DOF case we have an object that can be accelerated in the positive or negative direction due to frictional contact with a single finger. Based on a Coulomb friction coefficient of μ and a normal force f_N , the finger can resist a tangential force of μf_N before sliding. We assume the object has unit mass, so the maximum object acceleration is $a_o = \mu f_N$. We also assume the finger has a maximum acceleration of $a_f > a_o$. Additionally we define a finger acceleration a greater than 0 but less than a_o . The relationship between the accelerations can be written as $a_f > a_o > a > 0$.

Let $q_f(0) = q_o(0) = 0$ be the initial position of the finger and the object, and let $d_c(t) = q_f(t) - q_o(t)$ be the finger position relative to the object position at time t . The problem is to choose a finger acceleration profile $\ddot{q}_f : [0, T] \rightarrow \mathbb{R}$ to cause the object to slide relative to the finger by d_{goal} at time T , i.e., $d_c(T) = q_f(T) - q_o(T) = d_{\text{goal}}$.

A. Forward Dynamics

The forward dynamics problem is to determine the relative sliding acceleration \ddot{d}_c when given a finger acceleration \ddot{q}_f . If $\dot{d}_c \neq 0$, then $\ddot{d}_c = \ddot{q}_f - \text{sgn}(\dot{d}_c)a_o$. If $\dot{d}_c = 0$ and $|\ddot{q}_f| \leq a_o$, then no sliding will occur. If $\dot{d}_c = 0$ and $|\ddot{q}_f| > a_o$, then $\ddot{d}_c = \ddot{q}_f - \text{sgn}(\ddot{q}_f)a_o$.

B. Inverse Dynamics

The inverse problem is to determine the finger acceleration \ddot{q}_f that achieves a desired relative sliding acceleration \ddot{d}_c . If $\dot{d}_c = \dot{d}_c = 0$, no slip occurs so any $|\ddot{q}_f| \leq a_o$ is valid. If $\dot{d}_c = 0$ and $|\dot{d}_c| > 0$, then $\ddot{q}_f = \ddot{d}_c + \text{sgn}(\dot{d}_c)a_o$. If $\dot{d}_c \neq 0$, then $\ddot{q}_f = \ddot{d}_c + \text{sgn}(\dot{d}_c)a_o$.

C. Motion Planning

We assume the finger and object are initially at rest. We also require that the finger’s net displacement and velocity after the motion be zero. To achieve the sliding regrasp while satisfying these constraints, we first accelerate the finger with $\ddot{q}_f = a$ for time T_1 . We then apply the maximum negative acceleration $\ddot{q}_f = -a_f$ for time T_2 . Next we apply $\ddot{q}_f = a$ for time $T_3 + T_4 = T_{34}$. To achieve zero final displacement and velocity for the finger, we choose $T_1 = T_{34}$ and $\dot{q}_f(T_1) = -\dot{q}_f(T_1 + T_2)$.

During T_1 , \dot{d}_c is zero and $|\ddot{q}_f| \leq a_o$ so no relative motion occurs. During T_2 , $\ddot{q}_f < -a_o$ so relative sliding occurs.

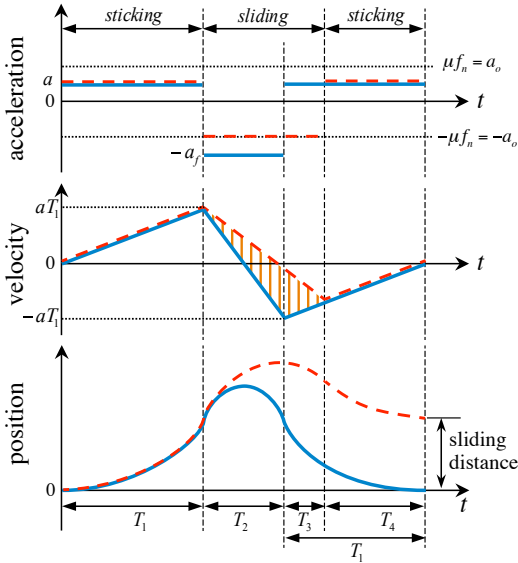


Fig. 1. A plot of the system motion profile of the 1-DOF problem. The blue curves represent the motion of the finger and the dashed red curves represent the motion of the object. The object has unit mass. In the velocity profile, the orange shaded area is the relative sliding distance.

During T_3 , $|\ddot{q}_f| \leq a_o$ but $\dot{d}_c \neq 0$ so sliding still occurs until $\dot{d}_c \rightarrow 0$. During T_4 , the object is sticking and \dot{d}_c is zero. Based on this analysis we assume three phases for each regrasp: an initial sticking phase (T_1), an intermediate sliding phase ($T_{23} = T_2 + T_3$), and a final sticking phase (T_4). The total time can be written as $T = T_1 + T_2 + T_3 + T_4$. The full series of accelerations, resulting velocities, and positions is shown in Fig. 1.

The total relative sliding distance d_{goal} is the integral between the finger and object velocity curves in the sliding phase. With given values of a_f, a_o, a and d_{goal} , we solve the following constraints to find the durations T_1, T_2 , and T_3 :

$$2aT_1 = a_f T_2, \quad (1)$$

$$a_o(T_2 + T_3) = a(2T_1 - T_3), \quad (2)$$

$$d_{\text{goal}} = -0.5(a_f - a_o)(T_2^2 + T_2 T_3). \quad (3)$$

Eq. (1) describes the finger velocity at time $T_1 + T_2$ by the symmetry assumption. Eq. (2) shows the object and finger velocities are equal at time $T_1 + T_2 + T_3$. Eq. (3) is the expression of the sliding distance. We can write the expressions for T_1, T_2, T_3 by solving (1), (2), (3) as

$$T_1 = \frac{a_f}{a} \sqrt{\frac{-d_{\text{goal}}(a + a_o)}{2(a + a_f)(a_f - a_o)}},$$

$$T_2 = \sqrt{\frac{-2d_{\text{goal}}(a + a_o)}{(a + a_f)(a_f - a_o)}}, T_3 = \sqrt{\frac{-2d_{\text{goal}}(a_f - a_o)}{(a + a_f)(a + a_o)}}. \quad (4)$$

D. Iterative Error Reduction

Following the execution of a planned repositioning trajectory, there will be some error in the actual displacement. This could be caused by inaccurate parameters,

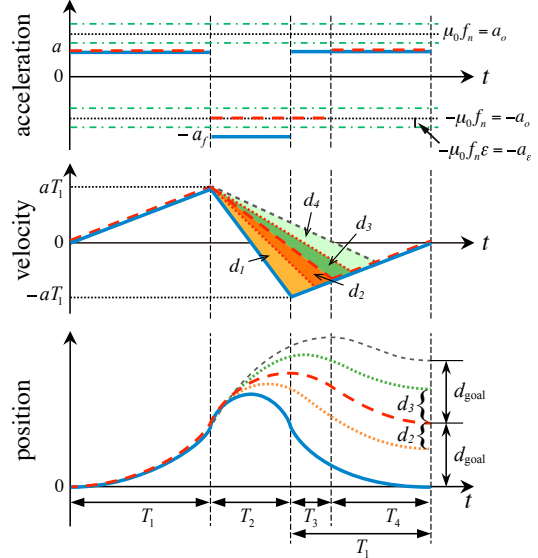


Fig. 2. The friction uncertainty affects the sliding distance. We denote d_1, d_2, d_3, d_4 as the areas of different triangles and $d_1 + d_2 = d_3 + d_4 = d_{\text{goal}}$. The areas d_2 and d_3 show the uncertainty in the sliding distance. Area d_2 represents the error when the friction coefficient is underestimated, and d_3 represents the overestimated case.

trajectory tracking error, or unmodeled dynamics. A significant source of error is an incorrect estimate of the friction coefficient μ . The following theorem shows that iterated execution of motion plans based on updated displacement information is sufficient to bring the object to the desired goal position d_{goal} in the presence of significant uncertainty in the friction coefficient.

Theorem 1: Consider the 1-DOF sliding regrasp system with a desired net sliding distance d_{goal} , a known constant normal force f_N , an estimated friction coefficient μ_0 , and an actual (unknown) constant friction coefficient $\mu \in [\mu_0(1 - \epsilon), \mu_0(1 + \epsilon)]$ for a friction coefficient uncertainty $\epsilon > 0$. Then by iterating the finger motion described above (where d_{goal} is recalculated at each iteration based on sensor data), the error in the net sliding distance converges asymptotically to zero with respect to the iterations provided $a < \mu_0 f_N(1 - \epsilon)$, $a_f > \mu_0 f_N(1 + \epsilon)$, and $a_f > \frac{f_N \mu_0 (a(1 + \epsilon) + (1 - \epsilon) f_N \mu_0)}{a + (1 - 2\epsilon) f_N \mu_0}$.

Proof: Without loss of generality, we prove the theorem for the case $d_{\text{goal}} < 0$, as indicated in Figure 2. With friction uncertainty included, the friction coefficient is $\mu \in [\mu_0(1 - \epsilon), \mu_0(1 + \epsilon)]$. The object acceleration can therefore be written as $a_{o,\text{actual}} \in [a_o - a_\epsilon, a_o + a_\epsilon]$, where $a_o = \mu_0 f_N$ and $a_\epsilon = \mu_0 f_N \epsilon$.

The sticking constraint in T_1 and T_4 is satisfied by the first condition $a < \mu_0 f_N(1 - \epsilon)$. The second condition, $a_f > \mu_0 f_N(1 + \epsilon)$, ensures that the object slides during the T_2 portion of the finger motion. The third condition ensures that the finger acceleration is large enough so that the object will not slide greater than $2d_{\text{goal}}$ during the sliding phase. When the friction coefficient is underestimated, the maximum sliding distance error caused by the friction uncertainty is the area of the orange triangle d_2 in Fig. 2, and can be expressed as:

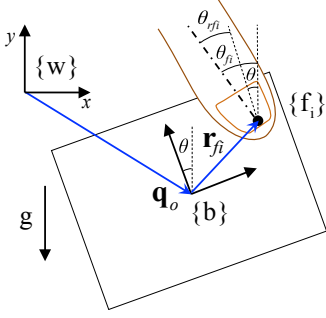


Fig. 3. Side view of an object in a two-fingered pinch grasp. $\{w\}$ represents the world frame, $\{b\}$ represents the body frame of the object, and $\{f_i\}$ represents the finger frame. The variables are defined in Section IV.

$$d_2 = \frac{-0.5a_\varepsilon(a + a_f)(T_2^2 + T_2T_3)}{a + a_o + a_\varepsilon}. \quad (5)$$

For the case where the friction coefficient is overestimated, the maximum sliding distance error is the area of the green triangle d_3 in Fig. 2, and can be expressed as

$$d_3 = \frac{-0.5a_\varepsilon(a + a_f)(T_2^2 + T_2T_3)}{a + a_o - a_\varepsilon}. \quad (6)$$

The range of the actual sliding distance can be written as $d_{\text{actual}} \in [d_{\text{goal}} - d_2, d_{\text{goal}} + d_3]$, and the error in sliding distance as $e = d_{\text{goal}} - d_{\text{actual}} \in [d_2, -d_3]$.

At each time step, the error e from the previous motion becomes the new d_{goal} and is used to replan a sliding motion. This is given as:

$$(d_{\text{goal}})_{i+1} = (d_{\text{goal}})_i - (d_{\text{actual}})_i \in [(d_2)_i, (-d_3)_i]. \quad (7)$$

From (3) and (5), when $a_f > \mu_0 f_N (1 + \varepsilon)$ we have

$$\frac{\|(d_2)_i\|}{\|(d_{\text{goal}})_i\|} < 1, \quad (8)$$

and from (3) and (6), when $a_f > \frac{f_N \mu_0 (a(1+\varepsilon) + (1-\varepsilon)f_N \mu_0)}{a + (1-2\varepsilon)f_N \mu_0}$ we have

$$\frac{\|(d_3)_i\|}{\|(d_{\text{goal}})_i\|} < 1. \quad (9)$$

By combining (7)-(9) we have $\left\| \frac{(d_{\text{goal}})_{i+1}}{(d_{\text{goal}})_i} \right\| < 1$. Let $k_i = \left\| \frac{(d_{\text{goal}})_{i+1}}{(d_{\text{goal}})_i} \right\|$, so $k_i \in [0, 1)$, and we can rewrite (7) as

$$\|(d_{\text{goal}})_{i+1}\| \in [-k_i \|(d_{\text{goal}})_i\|, k_i \|(d_{\text{goal}})_i\|],$$

which demonstrates that d_{goal} converges asymptotically to zero as the number of iterations increases. ■

IV. GENERAL PROBLEM STATEMENT

In this section we generalize the in-hand manipulation problem outlined in Section III for an n -fingered grasp, and define notation used in the rest of the paper.

We assume the object is held by n soft-finger contacts which are located on opposite sides of a laminar part moving in a vertical 2D plane. The sum of the normal forces at each contact must satisfy force balance at all instances so the object remains in the plane. We have controls on the acceleration of each finger, and the external forces to achieve

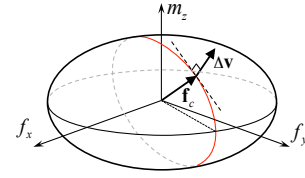


Fig. 4. Ellipsoid shape limit surface. Axes f_x , and f_y represent the tangential friction force and m_z represents the moment caused by the soft-finger contact. The sliding direction Δv is along the normal of the ellipsoid at the corresponding friction force vector f_c .

sliding come from gravity and the dynamic load on the object.

The frame $\{b\}$ is the body frame located at the CoM of the object, and $\{f_i\}$ is the frame located at each finger. All the configurations and velocities are defined with respect to the world frame $\{w\}$ unless noted otherwise. We denote the configuration of the object by its pose $\mathbf{q}_o = [x, y, \theta]^T$. The location of each of the n finger contacts is defined as $\mathbf{q}_{fi} = [x_{fi}, y_{fi}, \theta_{fi}]^T$, and the entire grasp is defined as $\mathbf{q}_f = [\mathbf{q}_{f1}, \dots, \mathbf{q}_{fn}]^T$. The relative positions between the object and the finger contacts are defined as $\mathbf{r}_{fi} = [x_{rfi}, y_{rfi}, \theta_{rfi}]^T$ where $\mathbf{q}_{fi} = \mathbf{q}_o + \mathbf{r}_{fi}$, and the relative position for the entire grasp is defined as $\mathbf{r}_f = [\mathbf{r}_{f1}, \dots, \mathbf{r}_{fn}]^T$. The configuration and velocity of the system are denoted as $\mathbf{q} = [\mathbf{q}_o, \mathbf{q}_f]^T$ and $\dot{\mathbf{q}} = [\dot{\mathbf{q}}_o, \dot{\mathbf{q}}_f]^T$. The full state of the system is defined as $[\mathbf{q}, \dot{\mathbf{q}}]^T$. Each finger contact normal force is represented by f_{Ni} defined in the finger frame $\{f_i\}$. The set of all finger normal forces is defined as $\mathbf{f}_N = [f_{N1}, \dots, f_{Nn}]^T$.

V. LIMIT SURFACES

In this section we discuss the concept of limit surfaces (LS) and how they are shaped given point contact and soft-finger friction models. Additionally we derive an expression for the frictional force from a soft-finger contact when given a relative velocity as well as an expression for the grasp limit surface given n individual limit surfaces.

A. Point Contact

A limit surface is defined as the boundary of the set of forces applied to an object that a contact can resist before the object starts sliding [9]. Based on the Coulomb friction model, a hard finger pressed against an object can only generate linear friction forces. Assuming isotropic friction, the limit curve for a point contact would be a circle centered about the origin where $f_x = f_y = \mu f_N$. Any external force \mathbf{f}_{ext} within this circle can be resisted. When \mathbf{f}_{ext} exceeds μf_N , a relative velocity Δv_l occurs in a direction normal to the LS and parallel to \mathbf{f}_{ext} .

B. Soft Finger

For a soft-finger model the contact area is no longer a point, and therefore linear as well as rotational forces can be resisted. The LS for a soft-finger contact can be approximated by an ellipsoid in the local contact force space f_x, f_y, m_z , and expressed in the world frame $\{w\}$ as shown

in Fig. 4 [10]. A mathematical representation of this ellipsoid is given by the following equation:

$$\mathbf{f}^T \mathbf{A} \mathbf{f} = 1, \quad (10)$$

where $\mathbf{f} = [f_x, f_y, m_z]^T$ represents an arbitrary friction force vector at the contact point and the matrix $\mathbf{A} \in \mathbb{R}^{3 \times 3}$ is a symmetric positive-definite matrix that determines the shape of the *LS* ellipsoid. In the general ellipsoid definition, $\mathbf{A} = \text{Diag}(s_1^{-2}, s_2^{-2}, s_3^{-2})$ where s_1, s_2 and s_3 represent the lengths of the semi-principal axes. We again assume isotropic dry friction so the maximum tangential force the contact can resist is $s_1 = s_2 = \mu f_N$. The maximum moment along the normal direction is $s_3 = ac\mu f_N$ where a is the radius of the contact patch and c is a constant from numerical integration. Here we take $c = 0.6$ based on findings in [10]. The radius of the contact patch depends on f_N , so each normal force f_{Ni} has a corresponding contact radius a_i .

When sliding happens, the contact force \mathbf{f}_c is on the *LS*, and the relative velocity is along the direction of the normal at that point (Fig. 4). Hence $\Delta \mathbf{v}$ and \mathbf{f}_c are not always parallel, but they always satisfy $\mathbf{f}_c \cdot \Delta \mathbf{v} \geq 0$, i.e., friction forces can only dissipate energy. Given a particular friction force \mathbf{f}_c and the ellipsoid it lies on, we can write the relative velocity $\Delta \mathbf{v}$ along the direction of the gradient of the ellipsoid with respect to \mathbf{f} at \mathbf{f}_c as

$$\Delta \mathbf{v} = \lambda \frac{\partial}{\partial \mathbf{f}} (\mathbf{f}^T \mathbf{A} \mathbf{f}) \Big|_{\mathbf{f}_c} \quad (11)$$

for some $\lambda \in \mathbb{R}$ which scales the normal vector to the relative velocity vector. When given a relative velocity, the corresponding friction force can be written as

$$\mathbf{f}_c = \frac{1}{\lambda} \mathbf{B} \Delta \mathbf{v}, \quad (12)$$

where $\mathbf{B} = \frac{1}{2} \mathbf{A}^{-1}$. Substituting (12) into (10) and utilizing $(\mathbf{A}^{-1})^T = \mathbf{A}^{-1}$, we have

$$\lambda = \frac{1}{2} \sqrt{\Delta \mathbf{v}^T \mathbf{A}^{-1} \Delta \mathbf{v}}. \quad (13)$$

Combining (12)-(13) we derive the function $\Gamma(\cdot)$ which gives the friction force vector as a function of a given relative velocity $\Delta \mathbf{v}$:

$$\mathbf{f}_c = \Gamma(\Delta \mathbf{v}) = \frac{\mathbf{A}^{-1} \Delta \mathbf{v}}{\sqrt{\Delta \mathbf{v}^T \mathbf{A}^{-1} \Delta \mathbf{v}}}. \quad (14)$$

C. Grasp Limit Surface

When there are multiple fingers on an object, the individual *LS* can be mapped to a consistent frame to generate the grasp limit surface (*GLS*). A reasonable choice of reference frame is the body frame $\{\mathbf{b}\}$ of the object. $\mathbf{G}_i(\mathbf{r}_{fi}) \in \mathbb{R}^{3 \times 3}$ is the map which relates the friction force at each contact to the wrench applied on the object. $\mathbf{G}_i(\mathbf{r}_{fi})$ depends on the contact's position relative to the object's CM and is defined as

$$\mathbf{G}_i(\mathbf{r}_{fi}) = \mathbf{G}_i = \begin{bmatrix} 1 & 0 & 0 \\ 0 & 1 & 0 \\ -y_{r_{fi}} & x_{r_{fi}} & 1 \end{bmatrix}. \quad (15)$$

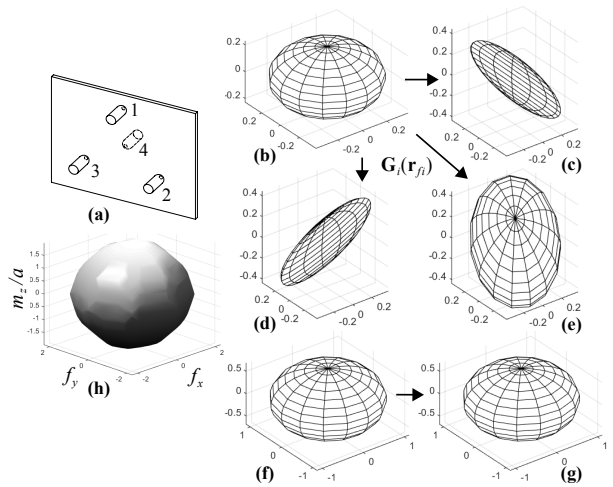


Fig. 5. This figure shows a 4-finger grasp and the resulting limit surfaces in the local finger frames, the body frame, and the composite grasp limit surface. (a) is a diagram of the grasp with three fingers on one side and one on the other. (b) is the identical limit surface for fingers 1-3 in the local finger frames. (c), (d), and (e) show the limit surfaces from fingers 1, 2, and 3 respectively mapped to the $\{\mathbf{b}\}$ frame using the \mathbf{G}_i transformation. (f) shows the limit surface for finger 4. Because it is located at the origin of $\{\mathbf{b}\}$ the mapping to $\{\mathbf{b}\}$ is the identity as shown in (g). (h) shows the composite grasp limit surface. The axes for (b)-(g) are all aligned and equivalent to the axes shown in (h).

The grasp limit surface is the convex hull of the sum of all possible friction forces that the grasp can resist. The *GLS* in the body frame can be expressed as

$$GLS = \delta \{ \mathbf{f} | \mathbf{f} = \sum_{i=1}^n k_i \mathbf{G}_i \mathbf{f}_i \ \forall \ \mathbf{f}_i \in LS_i \ \text{and} \ 0 \leq k_i \leq 1 \}, \quad (16)$$

where $\mathbf{f} = [f_x, f_y, m_z]^T$ is an arbitrary friction force on the *GLS*, LS_i is the limit surface for contact i , k_i is a scaling factor allowing forces inside LS_i , and \mathbf{f}_i is a friction force/torque set on the i^{th} limit surface.

Fig. 5 shows an example of a four-fingered grasp on an object and the resulting limit surfaces in the local contact frame expressed in $\{\mathbf{w}\}$, the common body frame $\{\mathbf{b}\}$, and the combined grasp limit surface expressed in $\{\mathbf{b}\}$.

VI. DYNAMICS

In this section we derive the sliding dynamics for the case where the object is sticking and when it is sliding. For this analysis it is assumed that the system state $[\mathbf{q}, \dot{\mathbf{q}}]^T$, the normal forces at each finger $f_{Ni}(t)$, and either the desired relative finger accelerations $\ddot{\mathbf{r}}_{fi}(t)$ or the finger accelerations $\ddot{\mathbf{q}}_{fi}(t)$ are given.

A. Sticking Dynamics

The object's dynamics are defined as

$$\mathbf{M} \ddot{\mathbf{q}}_o = \sum_{i=1}^n \mathbf{G}_i \mathbf{f}_i + \mathbf{g}, \quad (17)$$

where \mathbf{M} is the mass matrix of the object, \mathbf{f}_i is the friction force/torque set from each finger, and \mathbf{g} is the wrench on the object due to gravity. For the sticking case the frictional force at each contact is contained within the limit surface, i.e. $\mathbf{f}_i^T \mathbf{A}_i \mathbf{f}_i < 1$.

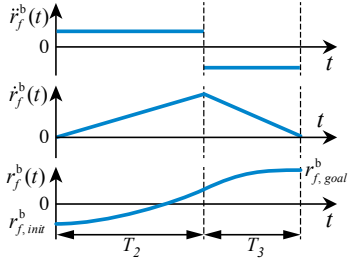


Fig. 6. A plot of the relative motion profile for 1-DOF.

B. Sliding Dynamics

When sliding is occurring, the relative velocity at each contact is defined as

$$\Delta \mathbf{v}_i = \dot{\mathbf{q}}_{fi} - \mathbf{G}_i^T \dot{\mathbf{q}}_o. \quad (18)$$

The forward dynamics problem is to determine the relative acceleration of each finger $\ddot{\mathbf{r}}_{fi}^b(t)$ when given the state of the system $[\mathbf{q}, \dot{\mathbf{q}}]^T$, the normal force vector $\mathbf{f}_{Ni}(t)$, and the acceleration of each finger $\ddot{\mathbf{q}}_{fi}(t)$. First we define the relative acceleration as

$$\ddot{\mathbf{r}}_{fi} = \ddot{\mathbf{q}}_{fi} - \ddot{\mathbf{q}}_o. \quad (19)$$

The dynamics in (17) can be rewritten as

$$\ddot{\mathbf{q}}_o = \mathbf{M}^{-1} \left[\sum_{i=1}^n \mathbf{G}_i \mathbf{f}_i + \mathbf{g} \right]. \quad (20)$$

Now combining (14), (18), (19), and (20), we can write the relative finger acceleration as

$$\ddot{\mathbf{r}}_{fi} = \ddot{\mathbf{q}}_{fi} - \mathbf{M}^{-1} \left[\sum_{i=1}^n \mathbf{G}_i \Gamma (\dot{\mathbf{q}}_{fi} - \mathbf{G}_i^T \dot{\mathbf{q}}_o) + \mathbf{g} \right]. \quad (21)$$

This equation allows us to calculate the relative sliding motion caused by given finger accelerations, and solves the forward dynamics problem.

The inverse problem is trivial, and (21) can easily be rearranged to solve for the required finger acceleration when given a desired relative sliding motion. For the inverse problem it is more convenient if we give the relative acceleration w.r.t. the body frame as the input. We denote $\ddot{\mathbf{r}}_{fi}^b$ as the relative acceleration w.r.t. the body frame $\{b\}$. We have

$$\mathbf{r}_{fi} = \mathbf{T}_i(\theta) \mathbf{r}_{fi}^b, \quad (22)$$

where $\mathbf{T}_i(\theta) \in SE(2)$ is the homogeneous transformation which maps \mathbf{r}_{fi}^b into \mathbf{r}_{fi} . Taking the first and second derivative with respect to time on both sides of (22) gives us

$$\dot{\mathbf{r}}_{fi} = \dot{\mathbf{T}}_i \mathbf{r}_{fi}^b + \mathbf{T}_i \dot{\mathbf{r}}_{fi}^b, \quad \ddot{\mathbf{r}}_{fi} = \ddot{\mathbf{T}}_i \mathbf{r}_{fi}^b + 2\dot{\mathbf{T}}_i \dot{\mathbf{r}}_{fi}^b + \mathbf{T}_i \ddot{\mathbf{r}}_{fi}^b.$$

VII. MOTION PLANNING

In this section we study the motion planning problem which can be stated as: given an initial state of the system and a desired relative configuration between the fingers and the object, find the finger trajectories and finger normal force profiles that realize the reconfiguration.

The general planning idea is inherited from the 1-DOF example in Section III. The planar finger motion has 3-DOFs

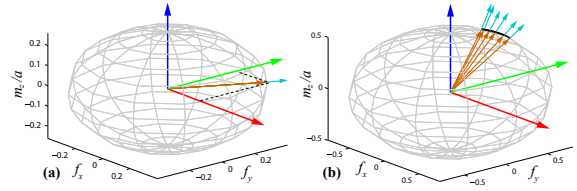


Fig. 7. Friction forces and corresponding relative velocities shown in the $\{f_i\}$ frame during the sliding phase. (a) is for the case in Section VIII-A, and (b) is for the case in Section VIII-B. The ellipsoid represents the limit surface LS . The brown arrows represent the friction force vectors \mathbf{f} , and the cyan arrows represent the corresponding relative velocities $\Delta \mathbf{v}$. The black curves are the trajectories of the friction force vectors on the LS during the sliding phase. In (a), the direction of $\Delta \mathbf{v}$ is constant in the sliding phase, so the trajectory of friction force on the LS is a point. The m_z axis is scaled by a factor of $1/a$ for display purposes.

and the frictional forces and sliding velocities are defined by the limit surface as discussed in Section V. For this analysis we assume that all fingers move the same way relative to the hand. The full repositioning motion consists of three phases; 1) *sticking*, 2) *sliding*, and 3) *sticking*. In the sticking phases the friction forces are contained within the limit surface so sliding does not occur, but in the sliding phase the forces lie on the limit surface and relative motions occur. Motion planning for the sticking phases simply involves choosing coupled finger/object accelerations that do not cause sliding, remain within the workspace, and achieve desired changes in the state.

For the sliding portion the motion planning problem must be solved for all fingers simultaneously to satisfy the limit surface force and acceleration constraints. Our proposed method for sliding phase motion planning is to choose a piecewise relative acceleration profile $\ddot{\mathbf{r}}_f^b(t)$ w.r.t. the object frame $\{b\}$ and times T_2 and T_3 for the accelerations to be applied. Once these parameters are defined, the motions of the fingers and the object can be calculated by the results from Section VI. An example of a proposed acceleration profile is shown in Fig. 6.

The accelerations in the sticking phases are also assumed to be constant. In the first phase the fingers accelerate the object to the initial sliding velocity $\dot{\mathbf{q}}_{o,is}$ in time T_1 . In the second phase, the finger slides on the object following the relative acceleration profile in time T_{23} . At the beginning of sliding we assume the relative velocity is along the direction of the desired relative acceleration at that instant to allow for the calculation of the friction force in (14). In the third phase the finger brings the object to rest with no sliding in time T_4 .

With all the assumptions above, the displacement of the finger is determined by the relative acceleration profile $\ddot{\mathbf{r}}_f^b(t)$, $\dot{\mathbf{q}}_{o,is}$, T_1 , T_{23} , T_4 . The motion planning problem is defined as choosing the above parameters to satisfy the workspace and robot joint-limit constraints.

VIII. SIMULATION

In this section we run simulations using the results from Sections VI and VII for the case where the object has only relative linear repositioning with no rotation, as well as

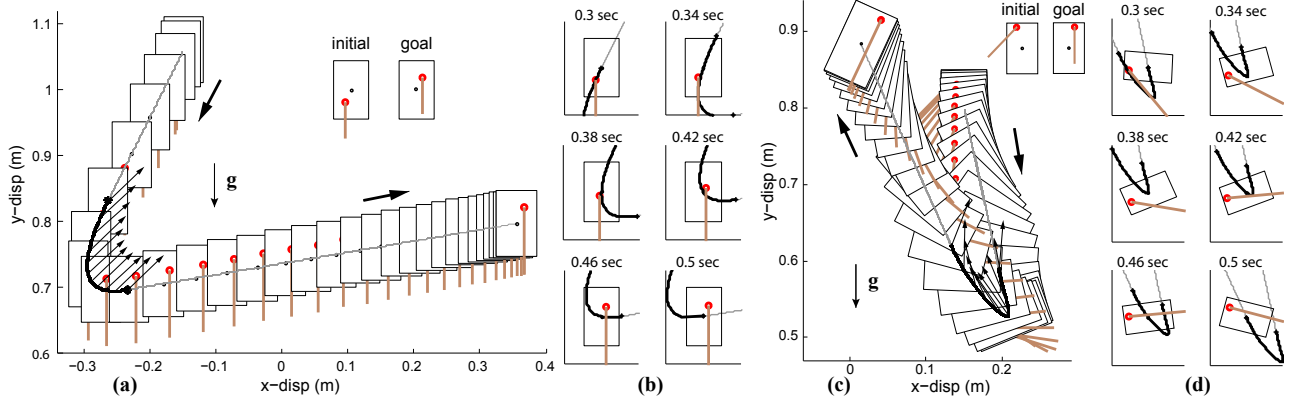


Fig. 8. Calculated trajectories of the system. The small red circles represent the finger contacts, and the brown lines represents the finger orientations. In (a) and (c) the solid gray curves are the object CoM trajectories. (a) and (b) are for the case with only linear relative motion. (c) and (d) are for the case with both linear and rotational relative motion. (b) and (d) show the motion during the sliding phase in more detail. The thick black curves show the sliding regions. The black arrows in the sliding regions represent the object linear acceleration directions during the sliding phase. The thick black arrows show the directions of the object motion.

the case where the object has relative linear and rotational repositioning with respect to the grasp. For this analysis we assume a two-point soft-finger pinch grasp of a rectangular extruded object moving in the vertical plane as shown in Fig. 3. We also assume that the normal force f_{Ni} for each finger is constant and of equal magnitude. Due to the symmetry of a pinch grasp, the contact is modeled as a single finger with twice the normal force. It is also assumed that $\dot{\mathbf{q}}_{init} = \dot{\mathbf{q}}_{final} = 0$. The robot workspace is a 1 m circle centered at the origin of the world frame. Note that in the following simulations, we only give the object's initial configuration as an input; the object's final configuration is determined by the motions of the three phases. The object is defined as a rectangle with a length of 0.1 m, width of 0.06 m, and a mass of 0.023 kg. The friction coefficient at the contact is 0.38.

A. Linear Relative Displacement

In this section we consider the case where only relative linear sliding in the x and y directions occurs. To achieve this we choose the direction of the relative acceleration so that it always intersects the CoM of the object. We give the initial relative position w.r.t. $\{b\}$ as $\mathbf{r}_{f,init}^b = [-0.01 \text{ m}, -0.02 \text{ m}, \pi \text{ rad}]^T$ and the goal relative position $\mathbf{r}_{f,goal}^b = [0.01 \text{ m}, 0.02 \text{ m}, \pi \text{ rad}]^T$. The normal force is 1.25 N and the radius of the contact patch is $a = 0.0174 \text{ m}$. The motion follows the same phase outline shown in Section VII, with the values $T_1 = 0.3 \text{ s}$, $T_{23} = 0.2 \text{ s}$, and $T_4 = 1.1 \text{ s}$. In the sliding phase, the relative acceleration w.r.t. $\{b\}$ is given as a piecewise profile

$$\ddot{\mathbf{r}}_f^b = \begin{cases} [2 \text{ m/s}^2, 4 \text{ m/s}^2, 0]^T, & 0.3 \text{ s} \leq t < 0.4 \text{ s} \\ [-2 \text{ m/s}^2, -4 \text{ m/s}^2, 0]^T, & 0.4 \text{ s} \leq t < 0.5 \text{ s}. \end{cases}$$

These values are chosen manually to satisfy the workspace, joint-limit, and acceleration constraints of the WAM arm. The sliding force for the linear case is shown in Fig. 7(a), and the resulting finger motion is shown in Fig. 8 (a) and (b).

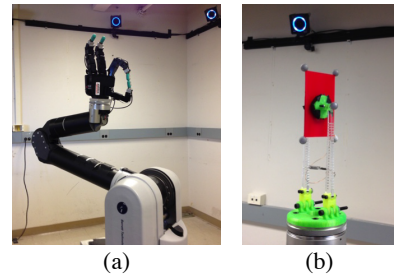


Fig. 9. (a) The ERIN instrumented manipulation environment, showing the 7-DOF WAM arm, the Allegro hand, four Syntouch biotac sensor fingertips, and part of the 10-camera OptiTrack high-speed tracking system. (b) The light-weight, spring-powered, constant normal force gripper.

B. Linear & Rotational Relative Displacement

This is a more general case where both linear and rotational relative repositioning occur. Initial relative position w.r.t. $\{b\}$ is given as $\mathbf{r}_{f,init}^b = [-0.01 \text{ m}, 0.04 \text{ m}, 0.75\pi \text{ rad}]^T$ and $\mathbf{r}_{f,goal}^b = [0.01 \text{ m}, 0.04 \text{ m}, \pi \text{ rad}]^T$. The normal force is 2.5 N and the radius of the contact patch is $a = 0.05 \text{ m}$. The times of the three phases are given as $T_1 = 0.3 \text{ s}$, $T_{23} = 0.2 \text{ s}$, and $T_4 = 0.3 \text{ s}$. In the sliding phase, the relative acceleration profile is manually chosen as:

$$\ddot{\mathbf{r}}_f^b = \begin{cases} [2 \text{ m/s}^2, 0, 25\pi \text{ rad/s}^2]^T, & 0.3 \text{ s} \leq t < 0.4 \text{ s} \\ [-2 \text{ m/s}^2, 0, -25\pi \text{ rad/s}^2]^T, & 0.4 \text{ s} \leq t < 0.5 \text{ s}. \end{cases}$$

The solved sliding friction force profile is shown in Fig. 7(b), and the object trajectory and the trajectory of the end of the finger are shown in Fig. 8(c) and (d).

IX. EXPERIMENT

In this section We tested the simulated trajectory from Section VIII-A using the ERIN instrumented manipulation environment shown in Fig. 9 (a). In this study, we used a light-weight spring-powered constant normal force gripper as shown in Fig. 9 (b). The gripper has a mass of 0.105 kg including the object. The control loop runs at 500 Hz, with vision feedback of the object and gripper poses at 360 Hz.

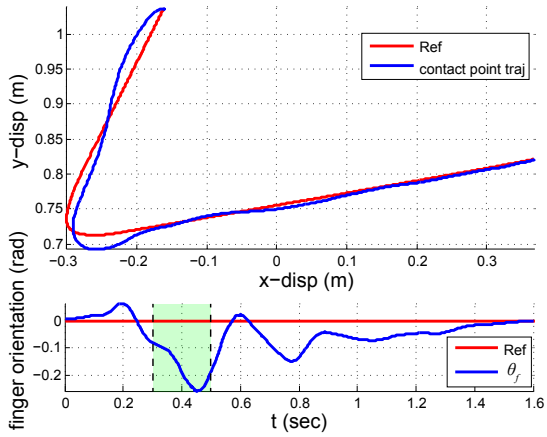


Fig. 10. Result of the WAM arm following a given trajectory. The green region marks the sliding phase.

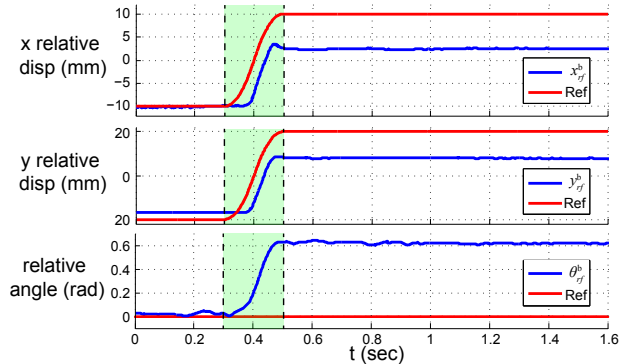


Fig. 11. Change of relative position w.r.t. the object frame \mathbf{r}_f^b . The green regions mark the sliding phase.

To test the simulation, the trajectory derived in Section VIII-A was given as a reference to the endpoint of the robot arm. By following this motion, we were able to reposition the object during the sliding phase. Fig. 10 shows how accurately the WAM arm followed the given reference trajectory. Fig. 11 shows how accurately the object followed the desired sliding motion \mathbf{r}_f^b . The simulations and the experimental results can be seen in the attached video.

We tested the consistency of the repositioning by repeating the experiment multiple times and the results are shown in Fig. 12. The experiment showed the same general sliding motion for each trial but with significant error in the final position. The mean error in $\mathbf{r}_{f,goal}^b$ was 1.03 cm with s.d. of 0.23 cm for x , 1.12 cm with s.d. of 0.4 cm for y , and -0.16 rad with s.d. of 0.27 rad for θ . This could have been caused by the robot trajectory tracking errors, and uncertainty in measured friction parameters, the gripper normal force, and the initial position.

X. CONCLUSION

In this paper, we presented a general framework for planning dynamic in-hand sliding manipulation motions and analyzed the dynamics for n -fingered grasp using soft-finger limit surface models. The framework was applied to the problem of a two-fingered grasp in the vertical plane. Two sliding motions were simulated by the proposed methods,

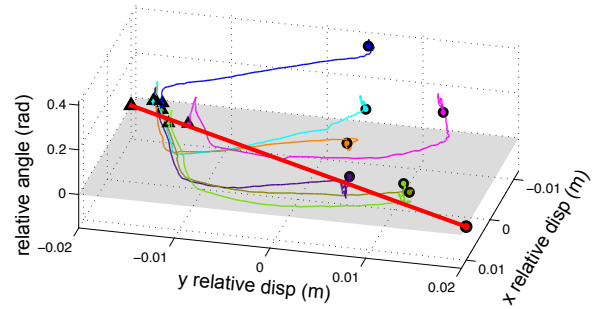


Fig. 12. Results of multiple trials plotted in the relative displacement space. The colored triangles show the initial relative position w.r.t. the object frame, and the colored circles show the final relative position for different trials. In every trial the robot followed the same reference trajectory. The red ones are desired reference values. The grey plane shows the zero relative rotation plane.

and one was validated experimentally. In future work we plan to implement feedback to improve the robustness of dynamic in-hand sliding manipulation. We propose the use of the iterative technique discussed in Section III-D for reducing error from uncertainty in measured friction parameters, the gripper normal force, and the initial position. We will also address controlled in-hand sliding manipulation for other grasp geometries and compliantly mounted fingers with force feedback. Furthermore we will improve the controller for the WAM arm to reduce trajectory tracking error.

REFERENCES

- [1] D. E. Whitney, "Quasi-static assembly of compliantly supported rigid parts," *Journal of Dynamic Systems, Measurement, and Control*, vol. 104, no. 1, pp. 65–77, 1982.
- [2] S. Huang and J. M. Schimmels, "Admittance selection for force-guided assembly of polygonal parts despite friction," *Robotics, IEEE Transactions on*, vol. 20, no. 5, pp. 817–829, 2004.
- [3] N. Chavan-Dafle, A. Rodriguez, R. Paolini, B. Tang, S. Srinivasa, M. Erdmann, M. T. Mason, I. Lundberg, H. Staab, and T. Fuhlbrigge, "Extrinsic dexterity: In-hand manipulation with external forces," in *IEEE International Conference on Robotics and Automation (ICRA)*, May 2014.
- [4] J. Trinkle and J. Hunter, "A framework for planning dexterous manipulation," in *Robotics and Automation, 1991. Proceedings., 1991 IEEE International Conference on*, Apr 1991, pp. 1245–1251 vol.2.
- [5] M. Yashima, Y. Shiina, and H. Yamaguchi, "Randomized manipulation planning for a multi-fingered hand by switching contact modes," in *Robotics and Automation, 2003. Proceedings. ICRA '03. IEEE International Conference on*, vol. 2, Sept 2003, pp. 2689–2694 vol.2.
- [6] D. Brock, "Enhancing the dexterity of a robot hand using controlled slip," in *Robotics and Automation, 1988. Proceedings., 1988 IEEE International Conference on*, Apr 1988, pp. 249–251 vol.1.
- [7] N. Furukawa, A. Namiki, S. Taku, and M. Ishikawa, "Dynamic regrasping using a high-speed multifingered hand and a high-speed vision system," in *Robotics and Automation, 2006. ICRA 2006. Proceedings 2006 IEEE International Conference on*, May 2006, pp. 181–187.
- [8] H. Arisumi, K. Yokoi, and K. Komoriya, "Casting manipulation midair control of a gripper by impulsive force," *Robotics, IEEE Transactions on*, vol. 24, no. 2, pp. 402–415, 2008.
- [9] S. Goyal, A. Ruina, and J. Papadopoulos, "Planar sliding with dry friction part 1. limit surface and moment function," *Wear*, vol. 143, no. 2, pp. 307–330, 1991.
- [10] N. Xydas and I. Kao, "Modeling of contact mechanics and friction limit surfaces for soft fingers in robotics, with experimental results," *The International Journal of Robotics Research*, vol. 18, no. 9, pp. 941–950, 1999.